

# Carrier Dynamics in Al-Rich AlGa<sub>N</sub>/AlN Quantum Well Structures Governed by Carrier Localization

Christian Frankerl,\* Felix Nippert, Marc Patrick Hoffmann, Christian Brandl, Hans-Jürgen Lugauer, Roland Zeisel, Axel Hoffmann, and Matthew John Davies

The carrier dynamics of Al-rich AlGa<sub>N</sub>/AlN quantum well (QW) structures in the presence of strong carrier localization is reported. Excitation density-dependent photoluminescence (PL) measurements at low temperatures reveal a clear correlation between the onset of efficiency droop and the broadening of the time-integrated PL spectra. While the droop onset is heavily impacted by the localization strength, the PL emission broadening is observed almost exclusively on the high energy side of the emission spectrum. Spectrally resolved PL decay transient measurements reveal a strong dependency of the carrier lifetimes on the emission photon energy across the spectrum, consistent with a distribution of localized states, as well as on the temperature, depending on the localization strength of the investigated structure. The characteristic “S”-shaped temperature dependence of the PL emission energy is shown to be directly correlated to the thermal redistribution of carriers between localized states. Based on these findings, the role of carrier localization in the recombination processes in AlGa<sub>N</sub> QW structures is underlined and its implications for efficiency droop are discussed.

efficiency (IQE) and efficiency droop, and is often regarded as possible cause for efficient light output despite high threading dislocation densities.<sup>[4–7]</sup> Composition and well width fluctuations create localized states, efficiently preventing carriers from reaching nonradiative recombination centers, thus diminishing losses and increasing the IQE. Characteristic fingerprints of carrier localization include, among others, the so-called “S”-shaped temperature dependence of the peak emission energy,<sup>[8]</sup> nonexponential photoluminescence (PL) decay transients,<sup>[9]</sup> and a strong dependency of the carrier lifetimes on emission photon energy.<sup>[10]</sup>

Recently, a similar effect was reported and studied in AlGa<sub>N</sub>-based epilayers and quantum wells (QWs), which generally suffer from a similar magnitude of TDDs compared with InGa<sub>N</sub>-based structures.<sup>[11–17]</sup>

Despite their continuing inferiority to blue LEDs, research efforts on AlGa<sub>N</sub>-based devices emitting in the deep ultraviolet (UV) spectrum have determined IQEs as high as  $\approx 65\%$ ,<sup>[18]</sup> significantly exceeding the maximum values expected by simple estimations based solely on the influence of the TDDs.<sup>[19]</sup> In a recent study, we have shown that the degree of carrier localization in AlGa<sub>N</sub>/AlN QWs is substantially larger than commonly reported in equivalent InGa<sub>N</sub>-based structures and directly affects the IQE and efficiency droop.<sup>[20]</sup>

In this article, we report on the recombination dynamics in AlGa<sub>N</sub>/AlN QW structures emitting in the UV-C spectral range by means of time-integrated and time-resolved, temperature- and carrier density-dependent PL spectroscopy. Our experiments enable us to directly trace the carrier density-induced and thermal redistribution of carriers between localized states and reveal its consequences for the recombination dynamics in the system, including efficiency droop, altogether highlighting the importance of carrier localization in AlGa<sub>N</sub>-based structures.


## 1. Introduction

Blue light-emitting diodes (LEDs) based on the InGa<sub>N</sub> material system have found widespread application into a multitude of commercial optoelectronic components.<sup>[1,2]</sup> Due to extensive research efforts, the efficiencies of such devices could be raised to very high standards.<sup>[3]</sup> In InGa<sub>N</sub>-based devices, the localization of carriers was demonstrated to heavily impact the optical properties of the active region, including the internal quantum

C. Frankerl, Dr. M. P. Hoffmann, C. Brandl, Dr. H.-J. Lugauer, Dr. R. Zeisel, Dr. M. J. Davies

OSRAM Opto Semiconductors GmbH  
Leibnizstr. 4, Regensburg 93055, Germany  
E-mail: Christian.Frankerl@osram-os.com

C. Frankerl, Dr. F. Nippert, Prof. A. Hoffmann  
Institut für Festkörperphysik  
Technische Universität Berlin  
Hardenbergstr. 36, Berlin 10623, Germany

 The ORCID identification number(s) for the author(s) of this article can be found under <https://doi.org/10.1002/pssb.202000242>.

© 2020 The Authors. Published by Wiley-VCH GmbH. This is an open access article under the terms of the Creative Commons Attribution License, which permits use, distribution and reproduction in any medium, provided the original work is properly cited.

The copyright line was corrected on 21 August 2020, after initial publication online.

DOI: 10.1002/pssb.202000242

## 2. Sample Structure and Measurement Methods

All QW structures studied in this article are grown on AlN templates on *c*-plane sapphire substrates using a standard metal–organic chemical vapor deposition (MOCVD) reactor. Additional growth details can be found in previous study.<sup>[20]</sup> Four samples are investigated in this article, two single-QW

(SQW) and two multi-QW (MQW) structures. The SQW samples were investigated recently in another work,<sup>[20]</sup> whereas the MQW samples were grown specifically for this study. The SQW samples are of similar Al content ( $\approx 50\%$ ) but varying QW width, and are labeled S25 (2.5 nm-thick QW) and S15 (1.5 nm-thick QW). Both SQW samples were also grown as equivalent MQW structures, consisting of five QWs separated by 8 nm-thick AlN barriers and are labeled M25 and M15, respectively. AlN barriers were used for reasons of homogeneous QW growth and to ensure comparability with the SQW structures.<sup>[21]</sup> The Al content of the MQW samples is slightly larger ( $\approx 53\%$ ) compared with the SQW samples, whereas the thicknesses are identical. On top of all structures, a 50 nm-thick AlN cap layer was deposited to avoid any surface effects, such as band bending due to Fermi-level pinning.<sup>[22]</sup>

Time-integrated PL measurements are conducted using a fifth harmonic Nd:YAG laser system ( $\lambda = 213$  nm,  $\tau = 1$  ns, and  $f_{\text{rep}} = 1$  kHz) and a closed-cycle helium cryostat with an operating range between 15 and 325 K. Carrier density-dependent measurements are carried out at  $T = 15$  K, whereas temperature-dependent “S”-shaped measurements use a low excitation power density of  $\approx 5$  kW cm<sup>-2</sup> to ensure a small occupation factor of the localized states. Time-resolved PL measurements are carried out using a Ti:Sa laser system ( $\lambda = 242$  nm,  $\tau = 2$  ps, and  $f_{\text{rep}} = 80$  MHz) and a continuous flow helium cryostat with an operating range between 5 and 350 K. The excitation power density of the Ti:Sa laser is held constant at  $\approx 50$  kW cm<sup>-2</sup> per pulse, indicating negligible contribution of droop. PL decay transients are recorded by the time-correlated single photon counting (TCSPC) technique. Due to the inherent nonexponentiality of the PL decay curves, as is discussed later in the article, carrier lifetimes are extracted by monoexponential fitting of the initial decay stage (typically the first few nanoseconds), yielding reasonable agreement

### 3. Experimental Section

In **Figure 1a**, the normalized time-integrated PL efficiency and full width at half maximum (FWHM) data of sample S25 at  $T = 15$  K are presented. The PL efficiency was calculated by

dividing the spectrally integrated PL intensity by the respective carrier density. The carrier density was numerically calculated by considering the laser spot size, the active volume of the QW and the measured carrier lifetimes at  $T = 5$  K, given that the used Nd:YAG laser system had a pulse length of a similar magnitude. It was observed that for carrier densities up to  $2 \times 10^{18}$  cm<sup>-3</sup>, the calculated PL efficiency was approximately constant. In this power region, spanning over more than two orders of magnitude and commonly labeled “plateau region,” the IQE was assumed to be close to unity due to negligible nonradiative recombination and quasi-resonant excitation of carriers into the QWs.<sup>[21]</sup> Increasing the carrier density further up to  $2 \times 10^{20}$  cm<sup>-3</sup>, a drastic decrease in PL efficiency by  $\approx 45\%$  is observed, representing the well-known efficiency droop.<sup>[10–18]</sup> Simultaneously, the FWHM of the PL spectrum was found to increase, closely correlating with the droop in PL efficiency. At carrier densities up to  $2 \times 10^{18}$  cm<sup>-3</sup>, corresponding to IQE  $\approx 100\%$ , the FWHM does not change significantly with carrier density.

In **Figure 1b**, a selection of the time-integrated PL spectra is illustrated, acquired at carrier densities in the plateau (red) and in the droop region (blue). In the plateau region of the PL efficiency, a variation of the carrier density did not change the shape of the emission. In contrast, the PL spectrum was significantly altered when the carrier density was high enough to induce droop, with a broadening of the spectrum emerging predominantly on the high energy side. When accounting for the simultaneous PL peak blue shift, it was found that indeed the shape of the low energy side of the spectrum remains practically unchanged, as shown in the inset of **Figure 1b**. An asymmetric broadening of the PL spectrum in the droop regime was reported previously in InGaN/GaN QW structures and ascribed to the delocalization of carriers,<sup>[10]</sup> which—as a consequence of their increased mobility—are more susceptible to nonradiative recombination.

As calculated in our previous study, carriers in sample S25 were subject to a carrier localization strength of  $\sigma = 49$  meV.<sup>[20]</sup> Recently, it was observed for elevated temperatures that the onset of efficiency droop scales with localization strength, with more strongly localized systems revealing droop at lower carrier densities.<sup>[15,20]</sup> To determine whether this finding also holds

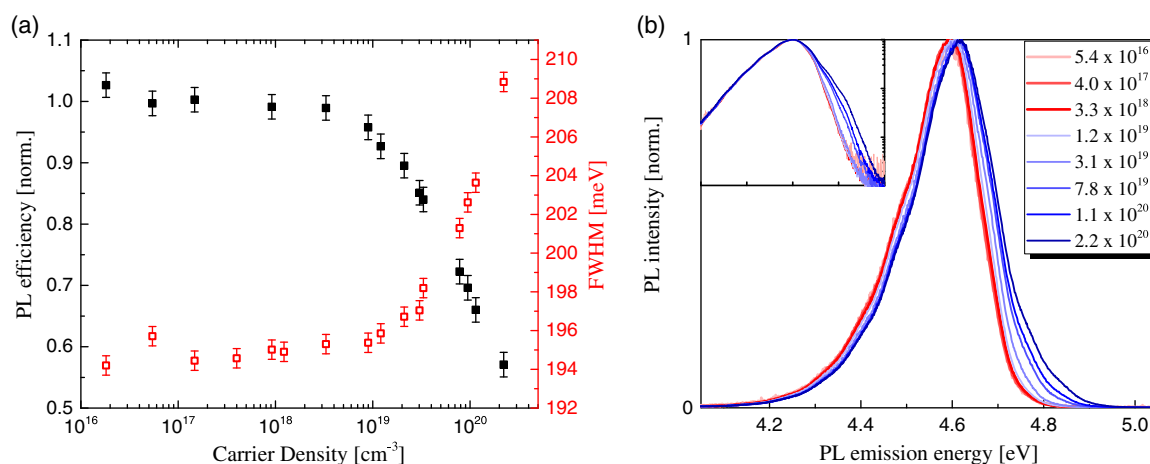


**Figure 1.** a) Normalized time-integrated PL efficiency (black squares) and FWHM (red dots) of sample S25 as a function of carrier density at  $T = 15$  K. b) Time-integrated normalized PL spectra recorded at varying carrier densities (in cm<sup>-3</sup>). Spectra in red and blue color shades indicate carrier densities before and in the droop regime, respectively. The inset shows the same data set, albeit peak shifted and on a logarithmic scale.

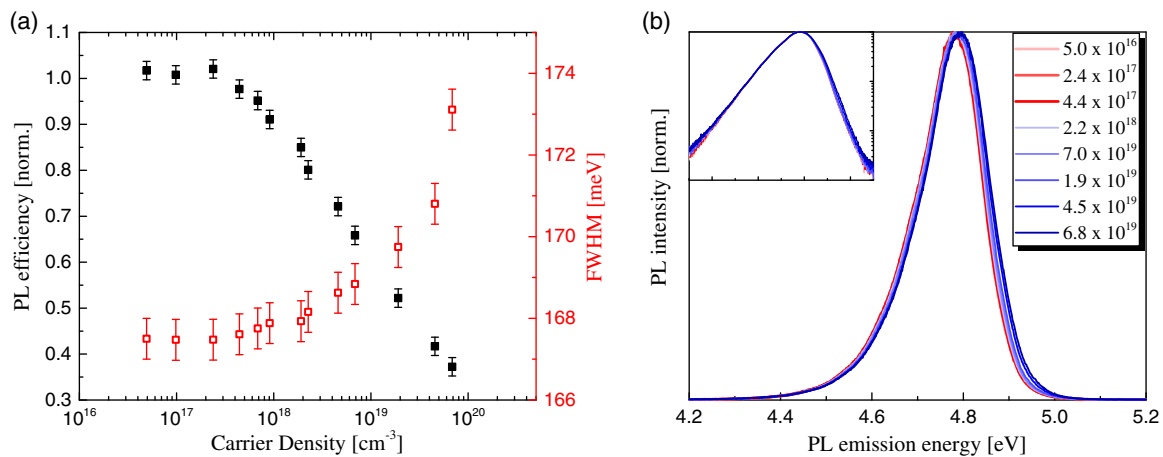


**Figure 2.** a) Normalized time-integrated PL efficiency (black squares) and FWHM (red dots) of sample S15 as a function of carrier density at  $T = 15$  K. b) Time-integrated normalized PL spectra recorded at varying carrier densities (in  $\text{cm}^{-3}$ ). Spectra in red and blue color shades indicate carrier densities before and in the droop regime. The inset shows the same data set, albeit peak shifted and on a logarithmic scale.

for low temperatures, **Figure 2a** shows the repetition of the carrier density-dependent PL efficiency measurements for sample S15, which was found to exhibit a significantly stronger localization of  $\sigma = 58$  meV.<sup>[20]</sup> Sample S15 already entered droop regime at a carrier density of  $3 \times 10^{17} \text{ cm}^{-3}$ , about an order of magnitude lower than the carrier density required to induce droop in sample S25, suggesting that droop onset was determined by localization strength at arbitrary temperatures. We emphasized that despite the drastically different carrier density required to cause droop in comparison with sample S25, the correlation between droop onset and asymmetric FWHM broadening is still evident in sample S15, as shown in **Figure 2a,b**. However, in comparison with sample S25, the FWHM broadening per unit PL efficiency reduction in sample S15 was smaller, with a less pronounced asymmetric broadening on the high energy side. The PL efficiency had dropped by almost 65% at the maximum achievable carrier density, which itself is about a factor of four lower than for sample S15 due to the heavily deviating carrier lifetimes. Thus, the structure with the larger carrier localization density is drastically more prone to efficiency droop.

Our previous findings highlight the need for a more detailed insight into the recombination dynamics in AlGaIn-based QW structures, which was accessible by time-resolved PL decay measurements. For this reason, such measurements were carried out on two MQW structures closely resembling the SQW structures discussed previously. MQW structures were studied as the rather low light output of SQW samples prohibits the acquisition of spectrally resolved PL decay transients due to insufficient signal-to-noise ratio. The slight difference in Al content results in a  $\approx 0.1$  eV shift in PL emission energies, but is not expected to significantly alter the carrier localization strength. In contrast, as we previously determined, the QW width seems to be the main parameter defining  $\sigma$ .<sup>[20]</sup> We confirm this by temperature-dependent PL measurements, which reveals the characteristic “S”-shaped dependence of the PL emission energy, as exemplarily shown in **Figure 3a** for sample M25. The data were normalized to the PL peak emission energy at 15 K, and the redshift region of the ‘S’-shape was fit by the commonly used equation<sup>[6,7,13,17]</sup>

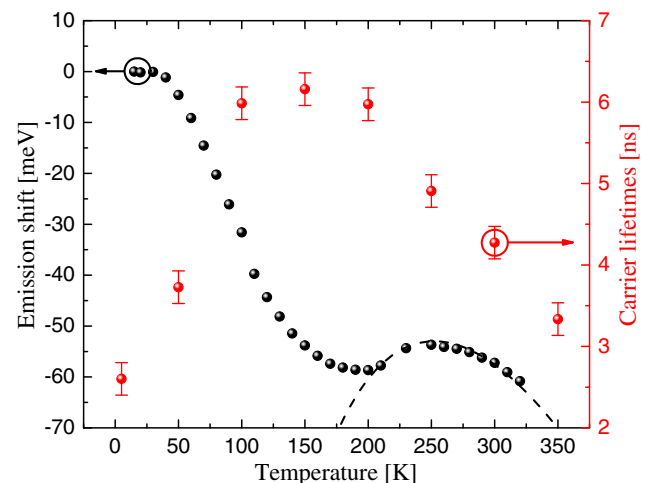


**Figure 3.** Comparison of the PL peak emission shift with the determined carrier lifetimes for sample M25. The dashed line is the fitting result via Equation (1).

$$E_{\text{peak}}(T) = E_g(0) - \frac{\alpha T^2}{\beta + T} - \frac{\sigma^2}{k_B T} \quad (1)$$

Here,  $E_g(0)$  is the bandgap at  $T = 0$  K,  $\alpha$  and  $\beta$  are the Varshni coefficients and  $\sigma$  reflects the carrier localization strength. The fitting result for sample M25 is shown as dashed line in **Figure 3a**. Extracted values for the carrier localization strengths are  $\sigma = 48$  meV for M25 and  $\sigma = 60$  meV for M15 (not shown), yielding almost identical localization strengths with respect to the SQW samples. **Figure 3a** also shows the extracted carrier lifetimes measured at the peak of the QW emission of sample M25 as a function of temperature. Analogous to what we recently observed in a SQW structure,<sup>[20]</sup> carrier lifetimes were found to monotonously increase until reaching a distinct maximum, and then decrease again. We stress the finding that the maximum carrier lifetime is obtained approximately at the temperature

of maximum PL peak emission redshift in all structures considered, an observation which is studied and explained in more detail later in the article.

**Figure 4** shows decay transients measured at various photon emission energies of sample M25, spanning across the entire PL spectrum. The induced carrier density was located in the plateau region, hence no contribution of efficiency droop was expected and the decay was expected to be purely radiative. As was typical for polar InGaN and AlGaIn QW structures, the PL decay transients were nonexponential and also did not follow a simple power law dependency, which would be expected for predominantly bimolecular recombination as proposed by the ABC model.<sup>[23]</sup> We also found that the decay transients cannot be fit satisfactorily using a stretched exponential and changing the excitation power density over more than one order of magnitude did not affect the decay shape. Hence, an interpretation in terms of partial and temporary screening of the internal electric field by an accumulation of electron–hole dipoles was excluded.<sup>[24]</sup> We further note that no fingerprints of excitonic recombination were observed. This finding was in agreement with numerical calculations of the polarization field in our MQW structures, which was estimated to be of the order of  $\approx 3$  MV cm<sup>-1</sup>, and thus was sufficiently large to efficiently dissociate excitons.<sup>[25]</sup> The timescale of the decay transients increased with decreasing emission photon energy, with the high energy side of the PL emission revealed a rapid reduction of the decay times. On the contrary, carrier lifetimes appeared to gradually saturate for low emission photon energies, with decay times differing by more than a factor of 3 across the whole PL emission spectrum. This overall behavior was interpreted in the context of carrier localization, with longer decay times attributed to carriers localized at deeper potential minima, hence recombining with smaller emission energy.<sup>[26]</sup> Vice versa, the fastest decay times were detected at the high energy side of the PL spectrum, representing carriers which are either weakly localized or fully delocalized.

In the inset of **Figure 4**, the decay transients are plotted on a “reduced timescale,” i.e., one in which the time axes of the decay

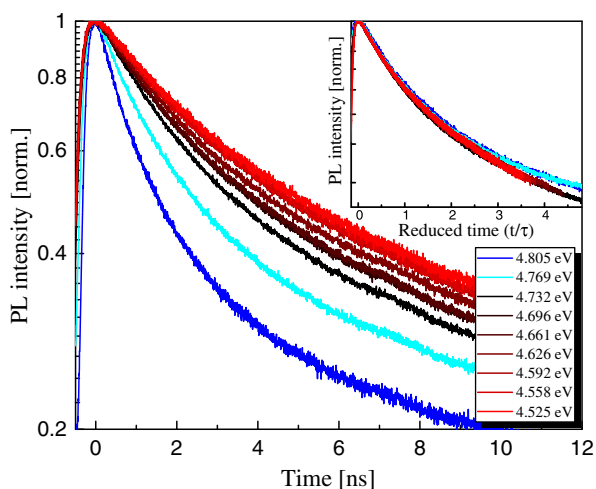


**Figure 4.** MQW PL decay transients at  $T = 5$  K of sample M25 detected at varying photon energies across the PL emission spectrum. The inset displays the same data set, albeit plotted on a “reduced timescale” (see text).

transients detected at different photon energies are normalized to their respective decay times.<sup>[26,27]</sup> With this approach, we found that one universal decay shape accurately described the PL time decay of all photon energies except for 4.769 and 4.805 eV. This finding strongly suggested that the vast majority of the PL emission originated from carriers localized among potential minima of varying depth, induced by local fluctuations of alloy composition and QW thickness, with the nonexponential decay shape reflecting the microscopic structure of the potential “landscape.”<sup>[26]</sup> The decay transients corresponding to photon energies of 4.769 and 4.805 eV follow a slightly different dependency, deviating in shape from the rest of the decay transients. Photons of these energies emerged from carriers recombining on the high energy side of the spectrum, supporting our interpretation that they were weakly localized or delocalized. Hence, the asymmetric broadening of the PL emission spectrum with increasing carrier density shown in **Figure 1** and **2** is attributed to the increasing influence of delocalized carriers, indirectly causing droop due to the promotion of nonradiative recombination.

Finally, we studied quantitatively the dependence of the extracted carrier lifetimes on detection photon energy at various temperatures for both samples M25 and M15. To evaluate the degree of (effective) carrier localization at different temperatures, we used the following equation put forward by Gourdon and Lavallard, which was widely used to extract the degree of localization in a structure from spectrally resolved PL transient measurements<sup>[28–32]</sup>

$$\tau(E) = \frac{\tau_{\text{rad}}}{1 + \exp\left(\frac{E - E_{\text{me}}}{E_0}\right)} \quad (2)$$

Here,  $\tau_{\text{rad}}$  is the radiative recombination lifetime of the most localized states,  $E_{\text{me}}$  is a characteristic energy related to the mobility edge energy, and  $E_0$  describes the density of the tail-state distribution, reflecting the effective degree of carrier localization. Three characteristic temperatures were chosen for closer analysis. These included the lowest and highest temperatures achievable by our continuous flow helium cryostat (5 and 325 K) as well as the temperature of maximum PL peak redshift, i.e., the minimum of the “S” shape, determined as 195 K (M25) and for 260 K (M15), respectively. The results—PL spectra, extracted carrier lifetimes and fittings via Equation (2)—are shown in **Figure 5**, whereas the corresponding values of  $\tau_{\text{rad}}$ ,  $E_{\text{me}}$ , and  $E_0$  are shown in **Table 1**.

At  $T = 5$  K, photoexcited carriers were distributed randomly among the in-plane potential landscapes of the QWs and do not possess enough thermal energy to escape the localized states they initially relaxed to. The extracted lifetimes are fit with Equation (2), yielding good agreement. We note several interesting observations here. First, as expected, the energy of the mobility edges was very high and located deep in the high energy side of the respective PL emission spectra. In a recent study, the energetic position of the mobility edge in InGaIn/GaN MQW structures was determined directly by a variation of the excitation photon energy, and was found to be significantly larger than the QW peak emission energy.<sup>[33]</sup> This finding coincided with our observation in AlGaIn-based MQWs and further underlined the similarity of the two material systems. Our results supported

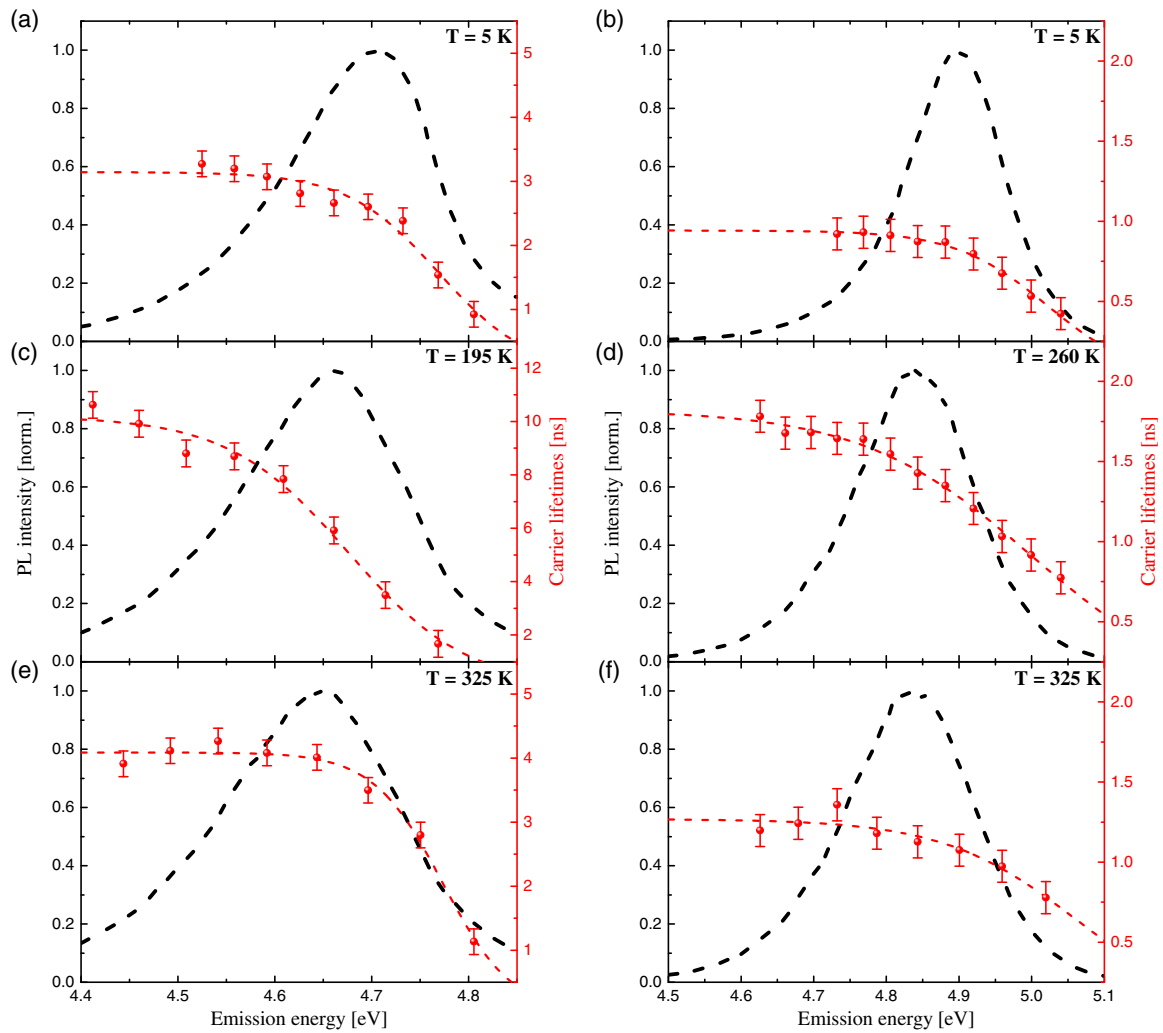


**Figure 5.** PL spectra and carrier lifetimes at for sample M25 at a)  $T = 5$  K, c)  $T = 195$  K, and e)  $T = 325$  K and sample M15 at b)  $T = 5$  K, d)  $T = 265$  K, and f)  $T = 325$  K. The dashed lines are the fitting results via Equation (2).

**Table 1.** Determined fitting parameters via Equation (2).

$T$ [K]	M25 ( $\sigma = 48$ meV)			M15 ( $\sigma = 60$ meV)		
	$\tau_{\text{rad}}$ [ns]	$E_{\text{me}}$ [eV]	$E_0$ [meV]	$\tau_{\text{rad}}$ [ns]	$E_{\text{me}}$ [eV]	$E_0$ [meV]
5	3.1	4.8	47	0.9	5.0	64
195/260	10.2	4.7	62	1.8	5.0	117
325	4.1	4.7	36	1.3	5.0	92

the hypothesis that the majority of the PL emission at low temperatures originated from localized carriers and suggested that the same assumption holds for elevated temperatures if the localization was strong enough. Furthermore, the extracted localization energies at low temperatures reasonably match the localization strengths determined by fitting of the “S”-shape temperature dependencies, illustrating the compatibility of both methods.

With increasing temperatures, carriers gradually gained thermal energy, allowing them to redistribute to deeper localized

states, resulting in a redshift of the PL emission energy. The maximum PL peak energy redshifts were obtained at  $T = 195$  K (M25) and  $T = 265$  K (M15), respectively. Thus, these temperatures corresponded to the carriers (on average) distributed among the deepest potential minima, which is already shown in Figure 3, where the maximum of the peak carrier lifetimes was found to coincide with the maximum redshift of the “S”-shaped PL peak temperature dependency. The dependence of the carrier lifetimes on detection photon energy further confirmed this interpretation, with carrier lifetimes varying heavily across the spectra. Both  $\tau_{\text{rad}}$  and  $E_0$  increased drastically for both samples, directly reflecting the thermal redistribution of carriers. Interestingly,  $E_{\text{me}}$  of M15 did not change with temperature, reflecting the continuing dominance of emission originating from localized carriers, whereas it reduced for M25. Finally, at  $T = 325$  K, as an increasing fraction of carriers had gained enough thermal energy to become delocalized, the carrier lifetime and effective localization strength of M25 recover, whereas the localization strength of M15 only decreased slightly and remained larger compared with  $T = 5$  K.

Based on the results presented in this article, we were able to propose responsible mechanisms for the observed carrier recombination dynamics. At low temperatures and low carrier densities, the PL emission of Al-rich AlGaN QWs originated primarily from carriers localized at potential minima of varying depth, similar to what has been reported in InGaN-based structures.<sup>[4,6–8,10]</sup> When the carrier density was increased beyond a threshold strongly depending on the localization strength, an increasing fraction of carriers was delocalized due to the gradual filling of the localized states. As the mobility of delocalized carriers was drastically increased, they were more prone to get captured at nonradiative recombination centers, decreasing the PL efficiency and giving rise to the well-known phenomenon of efficiency droop. The promotion of the carriers into weakly localized, higher-energy states was evidenced by the asymmetric broadening of the PL emission spectrum on the high energy side, correlating strongly with droop onset. The same correlation could also be observed in InGaN/GaN QWs.<sup>[10]</sup> Similarly, an increase in temperature caused the carriers to redistribute among the available potential minima, initially increasing their lifetime as they move into deeper, more strongly localized states. When the temperature approached room temperature, an increasing fraction of the carriers gained enough thermal energy to be able to leave their localized states and become delocalized, reducing both carrier lifetime and effective localization strength. The degree of localization strength  $\sigma$ , which could be reasonably estimated both by the temperature-dependent PL peak emission shift and low temperature time-resolved PL decay time measurements, determined the temperature at which thermal delocalization becomes effective.

#### 4. Conclusions

In conclusion, the presented time-resolved and time-integrated quasi-resonant PL measurements as a function of excitation power density and temperature provide a consistent picture of the carrier dynamics in AlGaN-based SQW and MQW structures governed by carrier localization. The asymmetric broadening of the PL spectrum in the droop regime is explained by the carrier density-induced filling of the localized states, enabling an increasing fraction of carriers to become delocalized. As a result, the mobility of the carriers increases, which renders them more susceptible for nonradiative recombination, in turn decreasing PL efficiency. Both the spectral dependence of the carrier lifetimes and the shift of the PL emission peak as a function of temperature are satisfactorily explained in the context of carriers localized among a potential fluctuation landscape. We observe a strong and nonmonotonic dependency of the carrier lifetimes on temperature as the carriers are redistributed into the lowest energetic states, correlating with the PL emission redshift. When the temperature is increased further, an increasing fraction of carriers is thermally delocalized, depending on the degree of localization strength  $\sigma$ . Our findings suggest that, similar to InGaN structures, carrier localization significantly influences the optical emission properties of AlGaN-based QW regardless of temperature and further highlights the need for a more detailed understanding of this effect.

#### Acknowledgements

A part of this work was funded by the German Federal Ministry of Economic Affairs (Bundesministerium für Wirtschaft und Energie) in the frame of the “Important Project of Common European Interest (IPCEI) on Microelectronics” (16IPCEI623). Furthermore, this work was supported by the German Federal Ministry of Education and Research (BMBF) within the “Advanced UV for Life” project (03ZZ0134A) and by the German Science Foundation (DFG) within the Collaborative Research Center 787 (CRC787). Open-access funding enabled and organized by Projekt DEAL.

#### Conflict of Interest

The authors declare no conflict of interest.

#### Keywords

AlGaN, carrier localization, carrier redistribution, efficiency droops, quantum wells, time-resolved photoluminescence

Received: April 24, 2020

Revised: June 30, 2020

Published online: August 7, 2020

- [1] A. A. Bergh, *Phys. Status Solidi A* **2004**, *201*, 12.
- [2] S. Pimputkar, J. S. Speck, S. P. DenBaars, S. Nakamura, *Nat. Photonics* **2009**, *3*, 180.
- [3] Y. Zhao, S. Tanaka, C.-C. Pan, K. Fujito, D. Feezell, J. S. Speck, S. P. DenBaars, S. Nakamura, *Appl. Phys. Express* **2011**, *4*, 082104.
- [4] S. Y. Karpov, *Phys. Status Solidi RRL* **2010**, *4*, 11.
- [5] J. Wang, L. Wang, W. Zhao, Z. Hao, Y. Luo, *Appl. Phys. Lett.* **2010**, *97*, 201112.
- [6] S. Hammersley, T. J. Badcock, D. Watson-Parris, M. J. Godfrey, P. Dawson, M. J. Kappers, C. J. Humphreys, *Phys. Status Solidi C* **2011**, *8*, 7.
- [7] S. Hammersley, D. Watson-Parris, P. Dawson, M. J. Godfrey, T. J. Badcock, M. J. Kappers, C. McAleese, R. A. Oliver, C. J. Humphreys, *J. Appl. Phys.* **2012**, *111*, 083512.
- [8] Y.-H. Cho, G. H. Gainer, A. J. Fischer, J. J. Song, S. Keller, U. K. Mishra, S. P. DenBaars, *Appl. Phys. Lett.* **1998**, *73*, 10.
- [9] V. J. Wang, S. J. Xu, D. G. Zhao, J. J. Zhu, H. Yang, X. D. Shan, D. P. Yu, *Opt. Express* **2006**, *14*, 26.
- [10] M. J. Davies, T. J. Badcock, P. Dawson, M. J. Kappers, R. A. Oliver, M. J. Kappers, C. J. Humphreys, *Appl. Phys. Lett.* **2014**, *102*, 022106.
- [11] G. Tamulaitis, J. Mickevičius, K. Kazlauskas, A. Žukauskas, M. S. Shur, J. Yang, R. Gaska, *Phys. Status Solidi C* **2011**, *8*, 7.
- [12] J. Mickevičius, G. Tamulaitis, M. Shur, M. Shatalov, J. Yang, R. Gaska, *Appl. Phys. Lett.* **2012**, *101*, 211902.
- [13] J. Mickevičius, G. Tamulaitis, M. Shur, M. Shatalov, J. Yang, R. Gaska, *Appl. Phys. Lett.* **2013**, *103*, 011906.
- [14] G. Tamulaitis, J. Mickevičius, J. Jurkevičius, M. S. Shur, M. Shatalov, J. Yang, R. Gaska, *Phys. B* **2014**, *453*, 40.
- [15] J. Mickevičius, J. Jurkevičius, G. Tamulaitis, M. S. Shur, M. Shatalov, J. Yang, R. Gaska, *Opt. Express* **2014**, *22*, A491.
- [16] J. Mickevičius, J. Jurkevičius, A. Kadys, G. Tamulaitis, M. Shur, M. Shatalov, J. Yang, R. Gaska, *J. Phys. D: Appl. Phys.* **2015**, *48*, 275105.
- [17] J. Mickevičius, J. Jurkevičius, A. Kadys, G. Tamulaitis, M. Shur, M. Shatalov, J. Yang, R. Gaska, *AIP Adv.* **2016**, *6*, 045212.
- [18] F. Nippert, M. Tollabi-Mazraehno, M. J. Davies, M. P. Hoffmann, H.-J. Lugauer, T. Kure, M. Kneissl, A. Hoffmann, M. R. Wagner, *Appl. Phys. Lett.* **2018**, *113*, 071107.

- [19] K. Ban, J.-I. Yamamoto, K. Takeda, K. Ide, M. Iwaya, T. Takeuchi, S. Kamiyama, I. Akasaki, H. Amano, *Appl. Phys. Express* **2011**, *4*, 052101.
- [20] C. Frankerl, F. Nippert, M. P. Hoffmann, H. Wang, C. Brandl, H.-J. Lugauer, R. Zeisel, A. Hoffmann, M. J. Davies, *J. Appl. Phys.* **2020**, *127*, 095701.
- [21] C. Frankerl, M. P. Hoffmann, F. Nippert, H. Wang, C. Brandl, N. Tillner, H.-J. Lugauer, R. Zeisel, A. Hoffmann, M. J. Davies, *J. Appl. Phys.* **2019**, *126*, 075703.
- [22] J. P. Ibbetson, P. T. Fini, K. D. Ness, S. P. DenBaars, J. S. Speck, U. K. Mishra, *Appl. Phys. Lett.* **2000**, *77*, 2.
- [23] S. Karpov, *Opt. Quantum Electron.* **2015**, *6*, 1293.
- [24] H. Haratizadeh, B. Monemar, P. P. Paskov, P. O. Holtz, G. Pozina, S. Kamiyama, M. Iwaya, H. Amano, I. Akasaki, *Phys. Status Solidi B* **2004**, *5*, 1124.
- [25] C. R. Haughn, G. Rupper, T. Wunderer, Z. Yang, N. M. Johnson, M. Wraback, G. A. Garrett, *Appl. Phys. Lett.* **2019**, *114*, 102101.
- [26] A. Morel, P. Lefebvre, S. Kalliakos, T. Taliercio, T. Bretagnon, B. Gil, *Phys. Rev. B* **2003**, *68*, 045331.
- [27] T. J. Badcock, P. Dawson, M. J. Davies, R. A. Oliver, M. J. Kappers, C. J. Humphreys, *Phys. Status Solidi C* **2014**, *11*, 3.
- [28] C. Gourdon, P. Lavallard, *Phys. Status Solidi B* **1989**, *153*, 641.
- [29] S. F. Chichibu, H. Marchand, M. S. Minsky, S. Keller, P. T. Fini, J. P. Ibbetson, S. B. Fleischer, J. S. Speck, J. E. Bowers, E. Hu, U. K. Mishra, S. P. DenBaars, T. Deguchi, T. Sota, S. Nakamura, *Appl. Phys. Lett.* **1999**, *74*, 10.
- [30] Y. Narukawa, Y. Kawakami, S. Fujita, S. Fujita, S. Nakamura, *Phys. Rev. B* **1997**, *55*, 4.
- [31] M. Baranowski, R. Kudrawiec, M. Syperek, J. Misiewicz, T. Sarmiento, J. S. Harris, *Nanoscale Res. Lett.* **2014**, *9*, 81.
- [32] T. Ozaki, M. Funato, Y. Kawakami, *Phys. Rev. B* **2017**, *96*, 125305.
- [33] W. E. Blenkhorn, S. Schulz, D. S. P. Tanner, R. A. Oliver, M. J. Kappers, C. J. Humphreys, P. Dawson, *J. Phys. Condens. Matter* **2018**, *30*, 175303.



Minerva Access is the Institutional Repository of The University of Melbourne

**Author/s:**

Frankerl, C; Nippert, F; Hoffmann, MP; Brandl, C; Lugauer, HJ; Zeisel, R; Hoffmann, A; Davies, MJ

**Title:**

Carrier Dynamics in Al-Rich AlGa<sub>N</sub>/AlN Quantum Well Structures Governed by Carrier Localization

**Date:**

2020-12-01

**Citation:**

Frankerl, C., Nippert, F., Hoffmann, M. P., Brandl, C., Lugauer, H. J., Zeisel, R., Hoffmann, A. & Davies, M. J. (2020). Carrier Dynamics in Al-Rich AlGa<sub>N</sub>/AlN Quantum Well Structures Governed by Carrier Localization. *Physica Status Solidi (B): Basic Research*, 257 (12), pp.2000242-2000242. <https://doi.org/10.1002/pssb.202000242>.

**Persistent Link:**

<http://hdl.handle.net/11343/281282>

**File Description:**

Published version

**License:**

CC BY